ARTICLE

Necroptosis mediators RIPK3 and MLKL suppress intracellular *Listeria* replication independently of host cell killing

Kazuhito Sai[1] ⓘ, Cameron Parsons[2], John S. House[3,4] ⓘ, Sophia Kathariou[2], and Jun Ninomiya-Tsuji[1] ⓘ

RIPK3, a key mediator of necroptosis, has been implicated in the host defense against viral infection primary in immune cells. However, gene expression analysis revealed that RIPK3 is abundantly expressed not only in immune organs but also in the gastrointestinal tract, particularly in the small intestine. We found that orally inoculated *Listeria monocytogenes*, a bacterial foodborne pathogen, efficiently spread and caused systemic infection in *Ripk3*-deficient mice while almost no dissemination was observed in wild-type mice. *Listeria* infection activated the RIPK3-MLKL pathway in cultured cells, which resulted in suppression of intracellular replication of *Listeria*. Surprisingly, *Listeria* infection–induced phosphorylation of MLKL did not result in host cell killing. We found that MLKL directly binds to *Listeria* and inhibits their replication in the cytosol. Our findings have revealed a novel functional role of the RIPK3-MLKL pathway in nonimmune cell-derived host defense against *Listeria* invasion, which is mediated through cell death–independent mechanisms.

Introduction

Receptor-interacting protein kinase 3 (RIPK3) is a serine/threonine protein kinase that mediates necroptosis, a programmed form of necrotic cell death. Upon induction of necroptosis, RIPK3 phosphorylates its downstream effector mixed lineage kinase domain-like (MLKL), which promotes oligomerization of MLKL on the plasma membrane, where it forms membrane pores to execute lytic cell death (Wang et al., 2014; Rodriguez et al., 2016). In cultured cells, combined stimulation with TNF, SMAC mimetic (an inhibitor of ubiquitin ligase cIAPs), and a pan-caspase inhibitor Z-VAD-FMK elicits necroptotic cell death through formation of a protein complex consisting of RIPK1, RIPK3, and MLKL (Linkermann and Green, 2014; Pasparakis and Vandenabeele, 2015). However, the physiological conditions that mimic such intricate stimulations are not yet clear. As neither *Ripk3*- nor *Mlkl*-deficient mice display overt abnormalities, the RIPK3-MLKL pathway is dispensable for physiological processes in tissue development and homeostasis (Newton et al., 2004; Wu et al., 2013). On the other hand, under a pathophysiological condition during virus infection, the RIPK3-MLKL pathway has been found to play an important role. Protein DNA-dependent activator of interferon regulatory factors (DAI, also known as ZBP-1) senses viral RNAs of influenza A virus and murine cytomegalovirus, which in turn interacts with RIPK3

through a unique protein–protein interaction motif called RIP homotypic interaction motifs domain to trigger necroptosis signaling (Upton et al., 2010; Thapa et al., 2016; Downey et al., 2017; Hartmann et al., 2017; Upton and Kaiser, 2017). This process mainly occurs in the front line of immune defense and limits virus spread by killing host immune cells.

The level of RIPK3 expression varies among cell types, making it a crucial determinant of whether the cells are capable of undergoing necroptosis. Multiple immune cells including monocytic leukemia and lymphocyte cell lines such as THP-1, Jurkat, and normal myeloid and lymphoid cells express high levels of RIPK3, which might reflect the role of RIPK3 in protection against virus invasion (Koo et al., 2015). Interestingly, colorectal cancer–derived cell lines such as HT-29 and Caco-2 cells also highly express RIPK3 despite the fact that most solid tumor–derived cells, e.g., HeLa, HepG2, and A549, completely lack its expression (Cai et al., 2014; Moriwaki et al., 2015; Su et al., 2016). Recent RNA-sequencing (RNA-seq) analyses as well as immunohistochemical staining in mice have also shown higher expression of *Ripk3* in the small intestine compared with other nonimmune organs (Newton et al., 2016; Wang et al., 2016). These facts suggest that RIPK3 possesses an important role in the gastrointestinal (GI) tract.

[1]Department of Biological Sciences, North Carolina State University, Raleigh, NC; [2]Department of Food, Bioprocessing, and Nutrition Sciences, North Carolina State University, Raleigh, NC; [3]Bioinformatics Research Center, North Carolina State University, Raleigh, NC; [4]Center for Human Health and the Environment, North Carolina State University, Raleigh, NC.

Correspondence to Kazuhito Sai: ksai@ncsu.edu; Jun Ninomiya-Tsuji: jtsuji@ncsu.edu.

Enteropathogenic bacteria, such as *Listeria monocytogenes* (hereafter referred to as *Listeria*), *Salmonella enterica*, and *Shigella* species., initially invade into intestinal epithelial cells to colonize and spread in the intestinal epithelium (Thiagarajah et al., 2015; Perez-Lopez et al., 2016). Multi-layered defense systems before and after cell invasion, including secretory IgA, antimicrobial peptides, pattern recognition receptors, and xenophagy, prevent their colonization within the intestinal epithelium and transmission to other organs (Ganz, 2003; Holmgren and Czerkinsky, 2005; Kawai and Akira, 2010; Sorbara and Girardin, 2015; Jo et al., 2016). In this study, we initially defined the expression levels of RIPK3 and MLKL in several organs. Their pronounced high-level expression in the intestinal epithelium led us to examine a potential role of RIPK3 and MLKL in the non-immune cell defense system against enteropathogenic bacteria.

Results

The RIPK3-MLKL pathway prevents systemic spread of *Listeria* in mice

To gain insight into the physiological role of RIPK3 signaling, we first analyzed its expression levels in human and mouse tissues. For expression analysis of *RIPK3* in multiple human tissues, we analyzed RNA-seq data obtained from the genotype-tissue expression (GTEx) databases (GTEx Consortium, 2013). As predicted by a higher abundance of RIPK3 in immune cells (Koo et al., 2015), the immune organs/tissues, such as spleen and blood, exhibit higher expression of *RIPK3*. Interestingly, we found that organs constituting the GI tract, including the esophagus, the small intestine, and the colon, also express *RIPK3* at higher levels (Fig. 1 A and Fig. S1 A). Similarly, we observed abundant expression of *MLKL* in the small intestine (Fig. S1 B). To further determine the tissue-specific protein levels of RIPK3 and MLKL, we collected mouse tissue extracts and performed Western blotting analysis. Consistent with the human transcriptional analysis, levels of RIPK3 protein were abundant in both the lymphoid tissue (spleen) and the duodenal enterocytes, less so in the liver, and were almost undetectable in the cerebral cortex (Fig. 1 B). We also found that MLKL protein was highly expressed in the small intestine, implying a potential importance of the RIPK3-MLKL pathway in digestive organs (Fig. 1 B). Furthermore, RIPK3 and MLKL proteins were abundant both in the duodenal- and ileal-enterocytes, suggesting their functional role throughout the epithelium of the small intestine (Fig. 1 C). Since the epithelium of the GI tract is the primary target of enteropathogenic bacteria invasion, we investigated the role of the RIPK3-MLKL pathway in protection against infection by foodborne bacteria. We used *Listeria*, a gram-positive intracellular bacterium that causes listeriosis and is widely used as a model pathogen for intracellular infection in the intestinal epithelium (McLauchlin et al., 2004; Lecuit, 2007). *Listeria* enters into enterocytes through internalins-mediated mechanisms (Schubert et al., 2002; Niemann et al., 2007). When successfully colonizing in the small intestine, *Listeria* travels to the liver through the portal vein and colonizes within the liver, which is the most prominent pathway of *Listeria* systemic infection (Lecuit et al., 2001; Melton-Witt et al., 2012). To test whether RIPK3 has a role in the intestinal barrier against *Listeria* infection, *Ripk3*-deficient and littermate

control mice were orally infected with *Listeria*, and *Listeria* burden in the liver at 3 d after infection was measured. While almost no liver colonization was observed in the control mice in our experimental settings, pronounced colonization of *Listeria* was observed in the liver of *Ripk3*-deficient mice (Fig. 1, D and E), indicating impairment of the innate immune barrier in these mice. We found that *Mlkl*-deficient mice also exhibited increased susceptibility to liver colonization of *Listeria* (Fig. 1 F). We note that the *Listeria* burden in the liver of *Mlkl*-deficient mice was less than that in the liver of *Ripk3*-deficient mice. These results imply that, although the RIPK3-MLKL pathway is important for preventing systemic spread of *Listeria*, RIPK3 has MLKL-independent innate immune functions that also contribute to the protection against *Listeria* infection. Recent studies have shown that RIPK3 promotes inflammatory cytokine production independently of MLKL activation and necroptosis (Lawlor et al., 2015; Najjar et al., 2016; Daniels et al., 2017), which is likely to cause the diminished protection against *Listeria* in *Ripk3*-deficient mice compared with *Mlkl*-deficient mice. Additionally, RIPK3-dependent autophagy, which does not require MLKL, might help to reduce *Listeria* burden in *Mlkl*-deficient mice (Harris et al., 2015).

The RIPK3-MLKL pathway inhibits intracellular replication of *Listeria*

The hyper-susceptibility of *Listeria* invasion can be mediated by a number of different mechanisms. Among them, we focused on *Listeria* entry and replication in enterocytes, since RIPK3 and MLKL are highly expressed in the intestinal epithelium. WT HeLa cells, which are deficient for RIPK3 expression (Sun et al., 2012), and HeLa cells that stably express FLAG-tagged RIPK3 were used as an in vitro model system of nonphagocytic epithelial cells for testing the role of RIPK3 in *Listeria* invasion. We first asked whether the RIPK3-MLKL pathway is activated by intracellular invasion of *Listeria*. Phosphorylation of RIPK3, determined by the migration shift of RIPK3 on SDS-PAGE, was observed at 24 h post-infection (hpi), indicating its activation subsequent to *Listeria* invasion (Fig. 2 A). MLKL is activated via phosphorylation at Thr357 and Ser358 by RIPK3 (Wang et al., 2014). We found that *Listeria* infection resulted in increased phosphorylation of MLKL, and this increase was dependent on RIPK3 (Fig. 2 A). *Listeria*-induced activation of MLKL was also observed in colorectal cancer–derived HT-29 cells, which express endogenous RIPK3 (Fig. 2 B; Koo et al., 2015). These results indicate that *Listeria* infection activates MLKL in nonphagocytic epithelial cells through RIPK3. We then asked whether the RIPK3-MLKL pathway modulates *Listeria* entry and/or replication in the cytosol. To restrict *Listeria* replication only in the cytosol, gentamicin was added to cell culture medium, which kills *Listeria* in medium or attached to the cell surface (Havell, 1986). The number of cytosolic *Listeria* at 2 hpi was not altered by the presence of RIPK3, indicating that neither *Listeria* entry process nor initial replication is targeted by the RIPK3 pathway (Fig. S2 A). In contrast, intracellular replication of *Listeria* was decreased in RIPK3-expressing cells at 6 hpi, and was significantly suppressed by the presence of RIPK3 at 24 hpi (Fig. 2, C and D). A RIPK3 kinase inhibitor GSK′872 increased *Listeria* burden in RIPK3-expressing cells, indicating that growth
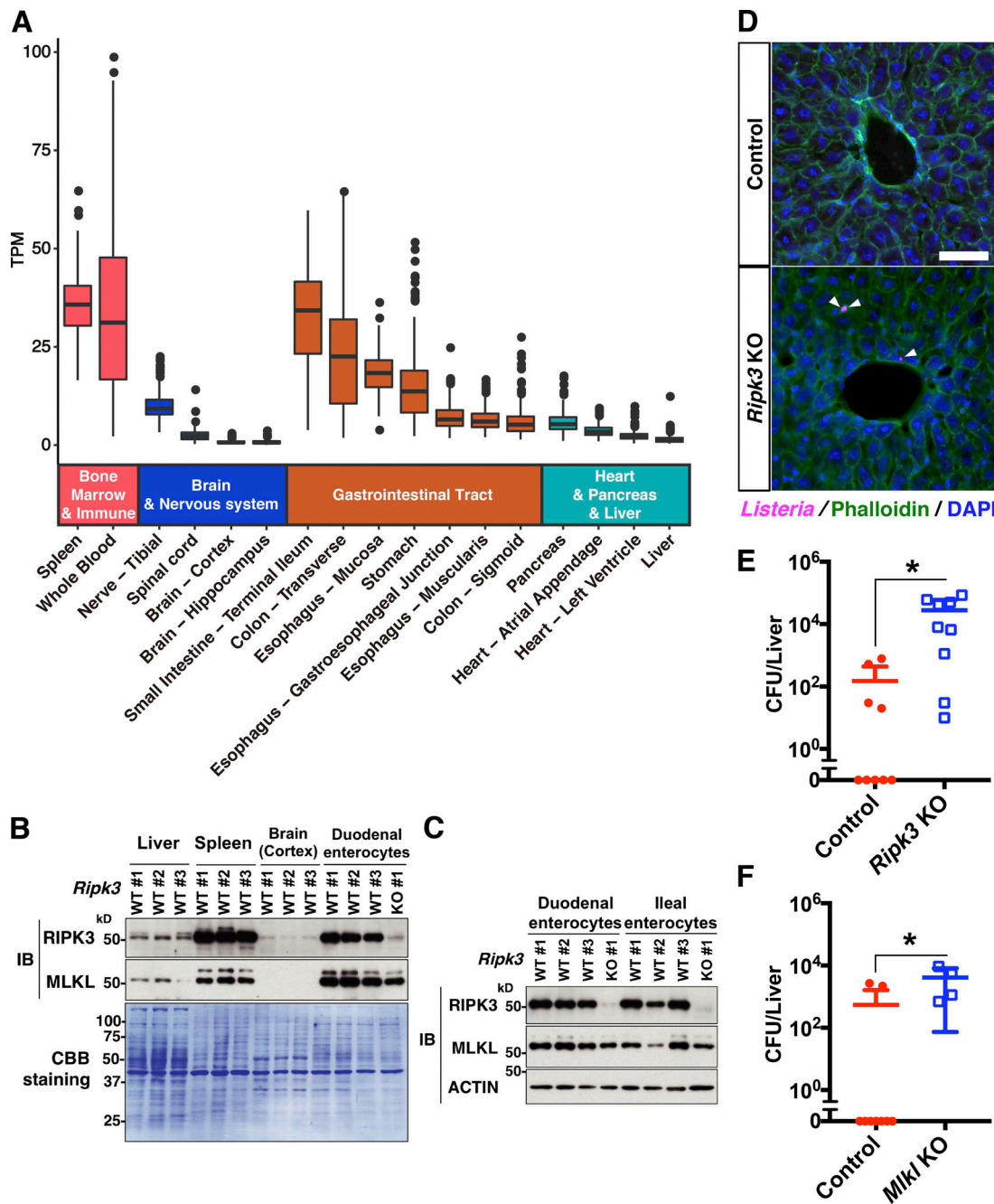
Figure 1. **RIPK3-MLKL pathway prevents systemic spread of *Listeria* in mice. (A)** Human expression levels by tissue for *RIPK3*. Gene-level transcripts per kilobase million (TPM) were downloaded from the GTEx portal and summarized across tissue type. Box and whisker plots are plotted in order of highest median expression to lowest. The bottom border, middle line, and top border of the box represent the first quartile, second quartile (median), and third quartile, respectively, while the lines represent 150% of the interquartile range. Outliers more than 150% of the interquartile range are represented as points. 17 representative tissues are shown (see Fig. S1 A for the full results). **(B and C)** Protein extracts of the indicated tissues from Ripk3+/+ (WT, #1–3) and Ripk3−/− (knockout [KO], #1) mice were analyzed by Western blotting with the indicated antibodies. Coomassie brilliant blue (CBB) staining of the whole membrane (B) and β-actin (C) were used as loading controls. **(D and E)** Ripk3−/− (KO) and littermate Ripk3+/+ or Ripk3+/− (control) mice were orally infected with *Listeria*. Immunofluorescence staining of liver-colonized *Listeria* (D) and CFU of *Listeria* in the liver (E) at 3 d after infection are shown. Arrowheads indicate *Listeria* in the liver. Bar, 50 µm (mean ± SEM; 6–9-wk-old; control, n = 9; Ripk3 KO, n = 9; *, P < 0.05). **(F)** Mlkl−/− (KO) and littermate Mlkl+/+ (control) mice were orally infected with *Listeria*. CFU of *Listeria* in the liver at 3 d after infection is shown (mean ± SEM; 6–9-wk-old; control, n = 9; Mlkl KO, n = 4; *, P < 0.05).

suppression by RIPK3 requires its kinase activity (Fig. 2 E). To determine whether MLKL participates in the *Listeria* growth suppression, we treated the cells with necrosulfonamide (NSA), a pharmacological inhibitor of MLKL (Sun et al., 2012). NSA

up-regulated *Listeria* growth in RIPK3 expressing HeLa cells and HT-29 cells but not in RIPK3-deficient HeLa cells (Fig. 2, F and G). Collectively, these results indicate that RIPK3 inhibits intracellular *Listeria* replication through phosphorylating
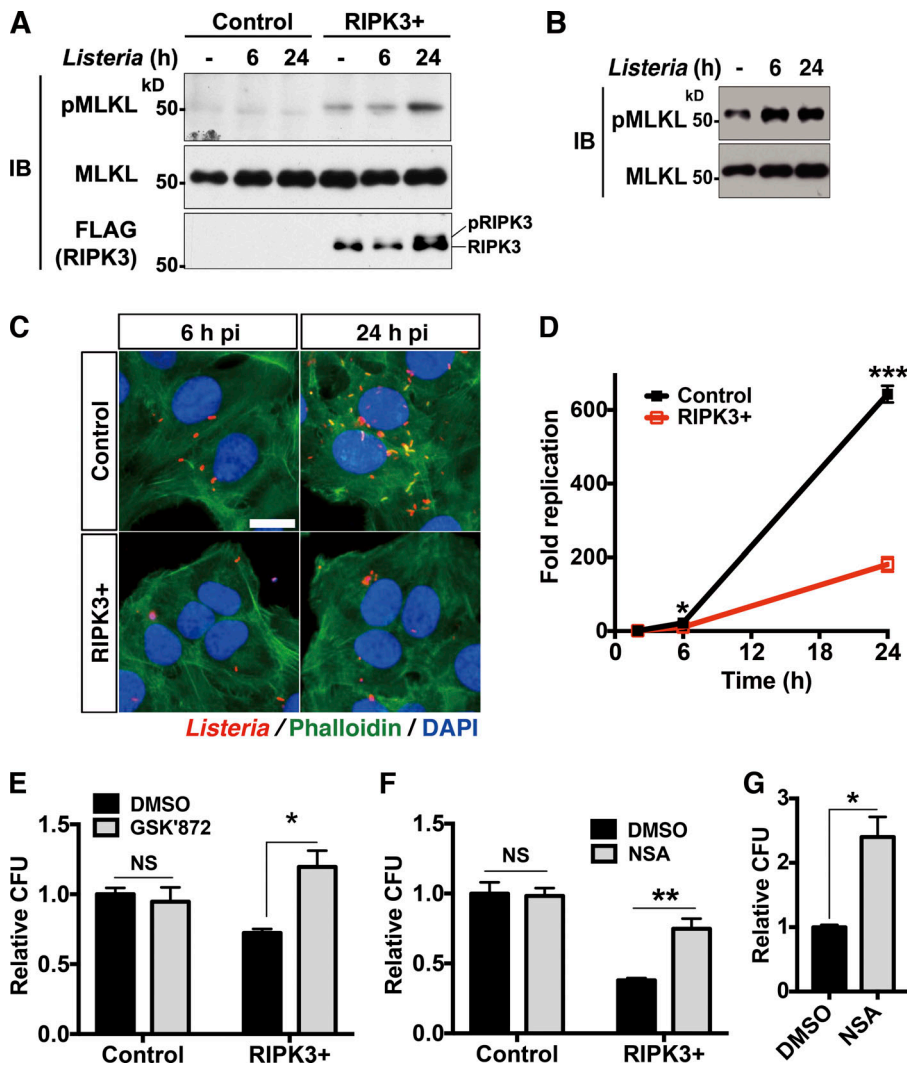
A

B

C

Listeria / Phalloidin / DAPI

D

E

F

G

Figure 2. **RIPK3-MLKL pathway suppresses intracellular replication of *Listeria*. (A and B)** Control, FLAG-tagged RIPK3 stably expressing (RIPK3+) HeLa cells (A), and HT-29 cells (B) were infected with *Listeria* (MOI of 10) and cultured for the indicated periods. Phosphorylation levels of MLKL (pMLKL) and RIPK3 (pRIPK3) were analyzed by Western blotting. Gentamicin was added to the culture to eliminate extracellular *Listeria*. **(C and D)** Control and RIPK3+ HeLa cells were infected with *Listeria* (MOI of 10) and cultured for the indicated periods. The cells were stained with anti-*Listeria* antibody, phalloidin, and DAPI at the indicated time point (C). Bar, 20 µm. Fold replication of *Listeria* (relative to the number of bacteria at 2 hpi) was measured (D). **(E)** Control and RIPK3+ HeLa cells were treated with either vehicle (DMSO) or 1 µM GSK'872 for 30 min. The cells were then infected with *Listeria* (MOI of 10) and cultured for 24 h with either DMSO or 1 µM GSK'872. *Listeria* CFU relative to vehicle-treated control is shown. **(F and G)** Control, RIPK3+ HeLa (F), and HT-29 cells (G) were treated with either vehicle (DMSO) or 1 µM NSA for 30 min. The cells were then infected with *Listeria* (MOI of 10) and cultured for 24 h with either DMSO or 1 µM NSA. *Listeria* CFU relative to vehicle-treated control is shown (mean ± SEM; $n = 3$; *, $P < 0.05$; **, $P < 0.01$; ***, $P < 0.001$).

MLKL. To further test if this pathway generally prevents intracellular bacteria growth, we infected WT and RIPK3-expressing HeLa cells with gram-negative bacteria *Salmonella typhimurium* (here after referred to as *Salmonella*). Although intracellular invasion of *Salmonella* induced RIPK3-dependent MLKL phosphorylation (Fig. S2 B), the presence of RIPK3 did not effectively suppress *Salmonella* growth in the cytosol (Fig. S2 C). These results suggest that the RIPK3-MLKL–mediated blockade of cytosolic bacterial growth is preferentially effective against certain types of intracellular bacteria.

Listeria-induced activation of the RIPK3-MLKL pathway does not kill host cells

Virus infection activates the RIPK3-MLKL pathway and kills infected cells through necroptosis, which protects the host from systemic virus spread (Upton et al., 2012; Thapa et al., 2016). Thus, we initially expected that the growth inhibition of *Listeria* by the RIPK3-MLKL pathway would be also mediated through a cell death–dependent mechanism. We confirmed that *Listeria* infection induces phosphorylation of MLKL at a level equivalent to TNF, SMAC mimetic, and a pan-caspase inhibitor Q-VD-OPh (TSQ) treatment (Fig. 3 A, top panel). Surprisingly, while TSQ

treatment killed a large population of the RIPK3-expressing cells, *Listeria* infection had almost no effect on cell viability (Fig. 3, B and C). To confirm that RIPK3-dependent cell lysis was not occurring in *Listeria*-infected cells, we performed the membrane permeability assay within the population of adherent cells. *Listeria* infection marginally induced membrane permeabilization in both RIPK3-negative and -positive cells, which is much less than that observed with TSQ treatment (Fig. 3 D). Consistent with the results obtained from cultured cells, no *Listeria*-invaded enterocytes showed signs of cell death in the both WT and *Ripk3*-deficient mouse small intestine after oral infection (Fig. S3). These results demonstrate that *Listeria* infection–induced MLKL activation does not elicit necroptotic cell death. To determine why *Listeria*-activated MLKL does not induce plasma membrane permeabilization of host cells, we tested two possibilities. One is that *Listeria* actively inhibits necroptotic cell death, and the other is that *Listeria* infection–induced activation of MLKL does not lead to its oligomerization, which is known to be required for translocation to the plasma membrane and permeabilization (Wang et al., 2014). To test the former possibility, we asked if the presence of intracellular *Listeria* suppresses necroptosis. We found that TSQ treatment
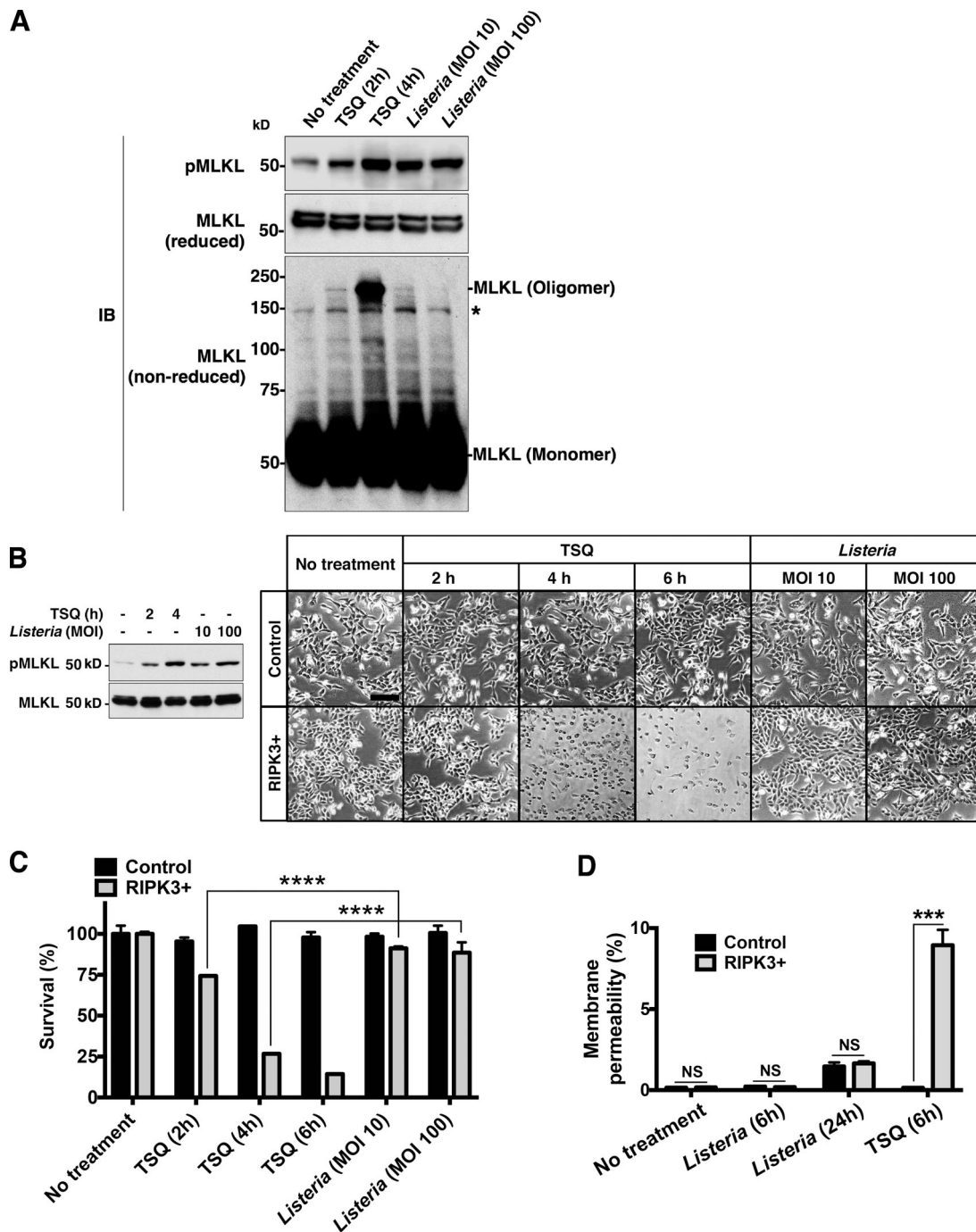
Figure 3.   *Listeria* invasion–induced phosphorylation of MLKL does not lead to necroptotic cell death. **(A)** FLAG-tagged RIPK3 stably expressing (RIPK3+) HeLa cells were either treated with 50 ng/ml TNF, 100 nM SMAC mimetic, 20 μM Q-VD-OPh (TSQ) for the indicated time periods, or infected with *Listeria* (MOI of 10 and 100) for 24 h. Phosphorylation (top panel) and oligomerization (bottom panel) of MLKL were analyzed by Western blotting. *, Nonspecific bands. **(B and C)** Control and RIPK3+ HeLa cells were either treated with TSQ for the indicated time periods, or infected with *Listeria* (MOI of 10 and 100) and cultured for 24 h. Phosphorylation level of MLKL (B, Western blotting), bright-field images of the cells (B, right panels), and cell viability measured by crystal violet staining (C) are shown. Bar, 200 μm. **(D)** Control and FLAG-RIPK3 stably expressing (RIPK3+) HeLa cells were either treated with TSQ or infected with *Listeria* (MOI of 100) and cultured for the indicated time periods. Floating dead cells were washed out after the culture. Membrane permeability of the remaining adherent cells was measured by incorporation of ethidium homodimer III (mean ± SEM; n = 3; ***, P < 0.001; ****, P < 0.0001).

killed both uninfected and *Listeria*-infected cells at the same rate (Fig. S4, A and B). To further confirm this observation, we used HeLa cells harboring doxycycline (Dox)-inducible NBB$_{140}$-2xFV fusion protein, an N-terminal fragment of MLKL conjugated

with 2xFV oligomerization cassette (N-terminal helix bundle and brace domain, NBB$_{140}$). This fusion protein forms oligomer through 2xFV domain upon dimerizer (DIM) treatment and induces necroptosis (Quarato et al., 2016). *Listeria* infection did not

inhibit DIM-induced cell death in NBB$_{140}$-2xFV–expressing cells (Fig. S4, C and D). Thus, it is unlikely that *Listeria* has the ability to block necroptotic cell death. We next asked whether *Listeria* infection induces MLKL oligomerization. Interestingly, while TSQ treatment induced MLKL oligomerization, no MLKL oligomer formation was observed in *Listeria*-infected cells (Fig. 3 A, bottom panel). These results indicate that *Listeria* infection activates MLKL with a unique state that does not induce its oligomerization, which is still effective in suppressing cytosolic *Listeria* replication.

MLKL directly binds to *Listeria* and inhibits their replication

RIPK3 phosphorylation of MLKL releases the N-terminal domain and promotes its binding to particular membrane phospholipids, namely phosphatidylinositol phosphates, through a four-helical bundle domain (Dondelinger et al., 2014). Interestingly, MLKL also possesses a strong binding affinity for cardiolipin, a unique phospholipid exclusively found on the mitochondrial inner membrane as well as bacterial cell membrane (Schlame et al., 2000; Zhang and Rock, 2008; Dondelinger et al., 2014; Wang et al., 2014). A peptidoglycan layer that composes the cell wall of gram-positive bacteria is accessible to molecules up to 57 kD (Demchick and Koch, 1996; Lambert, 2002). Various mammalian proteins, such as gasdermin D and septins, are known to be able to penetrate gram-positive bacterial cell walls and bind to the lipid membranes (Liu et al., 2016; Krokowski et al., 2018). Thus, we examined whether MLKL inhibits *Listeria* replication by directly targeting their lipid membranes. We first conducted fluorescence confocal microscopy analysis using HT-29 cells transiently expressing C-terminally FLAG-tagged MLKL. We found that MLKL was colocalized with *Listeria* in the cytosol at 6 hpi (Fig. 4 A). Consistent with the result showing *Listeria* infection does not trigger MLKL oligomerization, we did not observe localization of MLKL in the host plasma membrane during *Listeria* infection, while it was seen in TSQ-treated cells (Fig. S5 A). To further determine whether MLKL directly binds to *Listeria*, we performed an in vitro binding assay using NBB$_{140}$-2xFV protein, which does not require RIPK3 phosphorylation for its lipid binding and can be oligomerized by DIM treatment. We found that NBB$_{140}$-2xFV-VENUS but not VENUS alone bound to *Listeria* (Fig. 4 B). DIM treatment did not enhance the binding, confirming that oligomerization is not required for MLKL to target *Listeria* (Fig. 4 B). Contrary to gram-positive *Listeria*, we could not detect interaction between NBB$_{140}$-2xFV-VENUS and gram-negative bacteria, *Salmonella*, and *Escherichia coli* (Fig. S5 B). The selective binding ability of MLKL to gram-positive bacteria might be due to the differential lipid composition in their lipid membranes. Cardiolipin is less abundant in the gram-negative bacterial outer membrane compared with their inner membrane, which is not accessible for host proteins, or gram-positive bacterial membrane (Epand and Epand, 2009; Dalebroux et al., 2015). To ascertain whether MLKL directly inhibits replication of bacteria in a cell-free system, we incubated *Listeria*, *Salmonella*, and *E. coli* with cell lysates containing either VENUS alone or NBB$_{140}$-2xFV-VENUS for 2 h. Incubation of *Listeria* in NBB$_{140}$-2xFV-VENUS–containing lysates significantly reduced their number, and DIM treatment did not alter the efficiency of

growth inhibition (Fig. 4 C). These results demonstrate that MLKL monomer directly suppresses *Listeria* growth. As expected, NBB$_{140}$-2xFV-VENUS inhibits neither *Salmonella* nor *E. coli* growth in the culture (Fig. 4 C). We observed vacuolization in the cytosol of *Listeria* incubated with NBB$_{140}$-2xFV-VENUS, which is a hallmark of plasma membrane disruption caused by antimicrobial peptides (Fig. 4 D; Speert et al., 1979; do Nascimento et al., 2015). Our data demonstrate that the RIPK3-MLKL pathway suppresses intracellular *Listeria* growth through binding of MLKL to *Listeria*, which likely to disrupt their plasma membranes.

Discussion

To defend against invasion of enteropathogenic bacteria, organisms have evolved multi-layered defense systems. Toll-like receptors (TLRs) expressed on the surface of enterocytes and macrophages recognize pathogen-associated molecular patterns such as lipoteichoic acid, lipoprotein (TLR2 ligands), and lipopolysaccharide (TLR4 ligands), which lead to inflammatory responses to recruit immune cells for pathogen clearance (Kumar et al., 2009; Abreu, 2010). In phagocytic cells, bacteria-containing phagosomes are subjected to lysosomal degradation through multiple mechanisms including autophagy and LC3-associated phagocytosis (Sanjuan et al., 2007; Huang et al., 2009; Cemma and Brumell, 2012). In nonphagocytic enterocytes, bacteria enter the cells through mechanisms mediated by invasion-associated proteins such as internalins, and bacteria-containing vacuoles are targeted by autophagy adapters including p62, NDP-52, and optineurin, leading to lysosomal degradation (xenophagy; Thurston et al., 2012; Deretic et al., 2013; Bauckman et al., 2015). If bacteria successfully escape into the cytosol, they are recognized by nucleotide binding and oligomerization domain–like receptors, which elicits inflammatory responses (Meylan et al., 2006; Mariathasan and Monack, 2007). These defense systems are activated at the relatively early time point during infection (~4 hpi) and coordinately block bacterial cytosolic colonization (Philpott et al., 2000; McCaffrey et al., 2004; Travassos et al., 2010). In the present study, we have revealed a novel layer of defense against *Listeria* invasion by the RIPK3-MLKL pathway in epithelial cell types, which is activated later in the intracellular invasion process. The RIPK3-MLKL pathway modulated neither cell entry nor early colonization of *Listeria*, but suppressed their replication at 6–24 hpi (Fig. S2 A and Fig. 2, C and D). This implies that the RIPK3-MLKL–mediated defense functions to inhibit replication of pathogens that evade initial defense systems and have successfully started colonizing in the cytosol.

Our results have shown that the RIPK3-MLKL pathway does not induce necroptotic cell death but directly prevents replication of *Listeria* in epithelial cell types. However, *Listeria* infection is known to induce rapid necroptotic cell death in macrophages (Blériot et al., 2015; González-Juarbe et al., 2015). Macrophage death should be beneficial to protect the host by recruiting immune cells to effectively fight with pathogens. We speculate that, since macrophages express a broad range of pattern recognition receptors, they might use multiple bacterial-sensing systems that elicit necroptotic cell death. On the contrary, epithelial cells' ability to activate MLKL only for targeting cytosolic
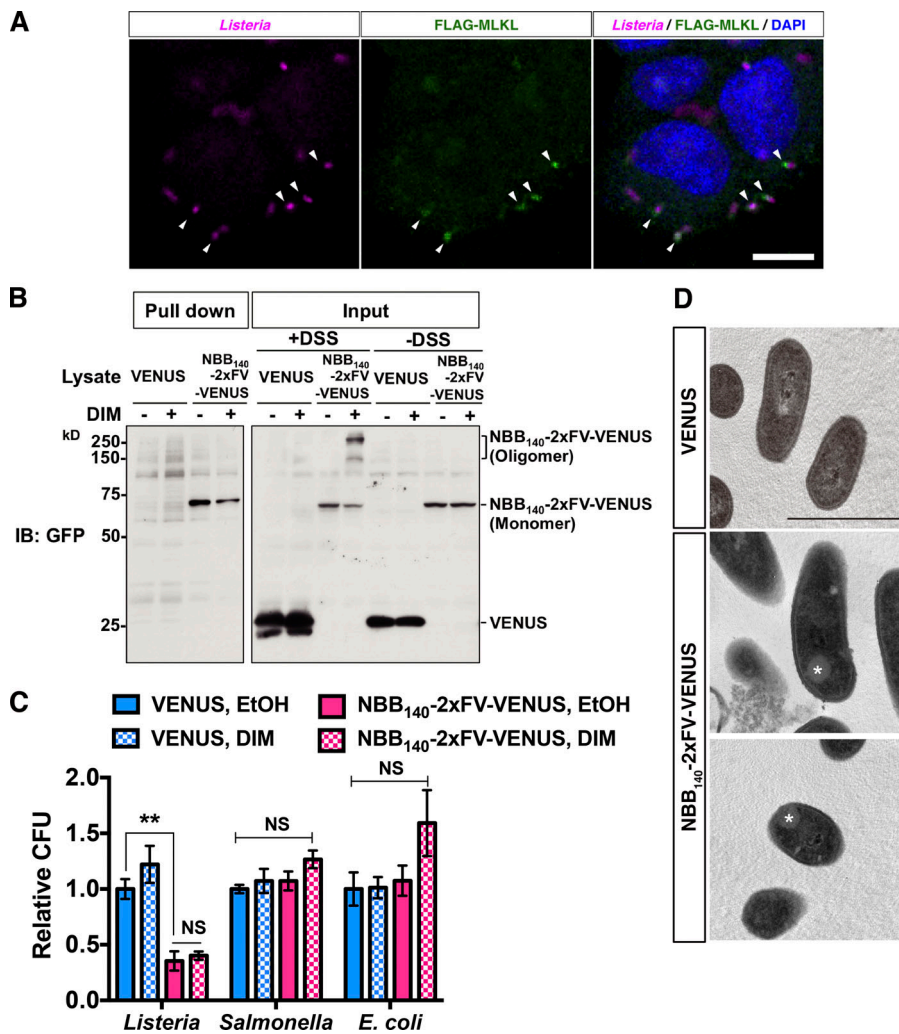
Figure 4. **MLKL directly binds to *Listeria* and inhibits their replication. (A)** HT-29 cells transiently expressing FLAG-tagged MLKL were infected with *Listeria* (MOI of 30) and cultured for 6 h. The cells were fixed and stained with anti-FLAG antibody and anti-*Listeria* antibody, and analyzed by confocal microscope. Arrowheads show the colocalization of MLKL with *Listeria*. Bar, 10 μm. **(B)** HeLa cell lysates containing either VENUS or NBB_{140}-2xFV-VENUS were treated with vehicle or DIM, and incubated with *Listeria* for 1 h. *Listeria*-bound NBB_{140}-2xFV-VENUS was detected by Western blotting. To determine the oligomerization state of NBB_{140}-2xFV in the presence and absence of DIM treatment, cell lysates were treated with a cross-linker disuccinimidyl suberate (+DSS). **(C)** HeLa cell lysates containing either VENUS or NBB_{140}-2xFV-VENUS were treated with vehicle (EtOH) or DIM, and incubated with the indicated bacteria for 2 h. Bacterial CFU relative to vehicle-treated, VENUS lysate sample is shown. (mean ± SEM; n = 6; **, P < 0.01). **(D)** HeLa cell lysates containing either VENUS or NBB_{140}-2xFV-VENUS were incubated with *Listeria* for 1 h. *Listeria* was fixed and analyzed by transmission EM. *, Vacuole-like structures formed by MLKL treatment. Bar, 1 μm.

bacteria but not their own plasma membrane should prevent disruption of the epithelial barrier in the intestine, which protects the host from highly problematic systemic invasion of pathogens. These cell type–dependent differential consequences of *Listeria*-induced activation of the RIPK3-MLKL pathway cooperatively contribute to the effective host defense.

The molecular mechanism by which cells sense cytosolic invasion of *Listeria* and activate the RIPK3-MLKL pathway remains unclear. A protein complex consisting of RIPK1, RIPK3, and MLKL has been reported to interact with autophagy machinery that is recruited to bacteria-containing phagosomes (Goodall et al., 2016). Thus, one possible mechanism is that induction of autophagy upon bacteria invasion also triggers the RIPK3-MLKL pathway to ensure effective clearance of the pathogens. Alternatively, cytosolic pattern recognition receptors that recognize bacterial moieties, such as NOD1/2 and TLR9, may be able to activate the pathway. Importantly, this MLKL activation does not kill host cells but does effectively block *Listeria* replication. In necroptosis, MLKL phosphorylation by RIPK3 leads to two separate processes: releasing the N-terminal domain for the translocation of MLKL in membranes, and MLKL oligomerization in the membranes. Both are essential for the formation of membrane pores that are reported to be permeable to up to 10-kD molecules (Xia et al., 2016). Given that

Listeria infection–activated MLKL suppresses *Listeria* growth without forming oligomers (Fig. 3 A and Fig. 4 C), MLKL phosphorylation by RIPK3 during *Listeria* infection seemingly causes only release of the N-terminal domain, which is sufficient for its anti-*Listeria* activity. The mechanisms by which MLKL is uniquely activated and recruited to *Listeria* warrant further investigation.

MLKL belongs to a large family of pore-forming proteins that include a complement (C9), cytotoxic granules (perforin and granulysin), a pyroptosis mediator (gasdermin D), and pro-apoptotic BCL2s (BAX and BAK), as well as a wide variety of antimicrobial peptides (Lieberman, 2003; Brogden, 2005; Youle and Strasser, 2008; Bischofberger et al., 2009; Wang et al., 2014; Ding et al., 2016). Like MLKL, granulysin and gasdermin D are associated with host programmed cell death upon pathogen invasion (Trapani and Smyth, 2002; Kayagaki et al., 2015). Interestingly, besides their effects on host cells, it has been recently reported that granulysin effectively kills intracellular pathogens, and that gasdermin D complex directly inhibits bacteria growth (Ernst et al., 2000; Walch et al., 2014; Liu et al., 2016). This raises the possibility that host-derived pore-forming proteins may follow a common evolutionary pathway to gain two different roles. One is direct interaction with pathogens, and another is induction of host cell killing, which effectively combat many types of pathogens.

Materials and methods

Antibodies, plasmids, and reagents

Anti–β-actin (AC15; Sigma-Aldrich), anti-*Listeria* (ab35132; Abcam), anti-mouse RIPK3 (R4277; Sigma-Aldrich), anti-MLKL (EPR17514; Abcam), anti-phospho-human MLKL (Thr357/Ser358; EPR9514; Abcam), anti-FLAG (M2; Sigma-Aldrich), and anti-GFP (GT859; GeneTex; 9F9.F9; Abcam) were used. FLAG-tagged human RIPK3 and C-terminally FLAG-tagged human MLKL plasmids were gifts from X. Wang (University of Texas Southwestern, Dallas, TX). NBB_{140}-2xFV-VENUS and control VENUS plasmids were gifts from D. Green (St. Jude Research Hospital, Memphis, TN). Plasmids were transfected using TransIT-X2 Reagent (Mirus Bio LLC). Alexa Fluor 488 phalloidin (Thermo Fisher Scientific), DAPI (Calbiochem), GSK'872 (Sigma-Aldrich), NSA (Calbiochem), TNF (PeproTech), Q-VD-OPh (TONBO Biosciences), SMAC mimetic (Brinapant; LC Laboratories), ethidium homodimer III (Biotium), Hoechst 33342 (Thermo Fisher Scientific), DIM (AP20187, Clontech), and disuccinimidyl suberate (Thermo Fisher Scientific) were used.

Mice and cell culture

Ripk3-deficient mice (C57BL/6) were obtained from V. Dixit (Genentech, San Francisco, CA; Newton et al., 2004). Since the protein levels of RIPK3 in the intestinal epithelium were not significantly different between *Ripk3* WT (+/+) and heterozygous (+/−) mice (Fig. S1 C), littermate and age-matched $Ripk3^{+/+}$ and $Ripk3^{+/−}$ mice were used as controls. *Mlkl*-deficient mice (C57BL/6) were obtained from J.M. Murphy (Walter and Eliza Hall Institute of Medical Research, Parkville, Australia; Murphy et al., 2013). Littermate and age-matched $Mlkl^{+/+}$ mice were used as controls. Inducible intestinal epithelium-specific *Tak1* knockout mice (*Villin-CreER*^{T2}, *Tak1*$^{flox/flox}$) were used as positive controls for TUNEL staining of the small intestine (Kajino-Sakamoto et al., 2010). All animal experiments were conducted with the approval of the North Carolina State University Institutional Animal Care and Use Committee.

HeLa (ATCC CCL-2) cells and HT-29 (ATCC HTB-38) cells were cultured in DMEM supplemented with 10% bovine growth serum (Hyclone) and 50 IU/ml penicillin-streptomycin at 37°C in 5% CO_2.

Bacterial strain and growth condition

L. monocytogenes serotype 1/2b strain 2011L-2858, implicated in a major outbreak of listeriosis via contaminated cantaloupe in 2011 (McCollum et al., 2013), *S. typhimurium* strain LT-2, and *E. coli* strain DH5a were used in the study. For making *Listeria* frozen stock cultures, *Listeria* was cultured in brain heart infusion (BHI) broth (BD Biosciences) at 37°C until the culture reached an OD_{600} of 0.8, and then 500-µl aliquots were stored at −80°C. Prior to each experiment, 500 µl of *Listeria* frozen stock culture was added to 9.5 ml of BHI broth and cultured at 37°C for 2 h. Prior to each experiment, *Salmonella* and *E. coli* were pre-cultured in LB broth at 37°C overnight. Then 500 µl of preculture was added to 9.5 ml of LB broth and cultured at 37°C for 2 h.

Establishing stable cell lines

FLAG-tagged human RIPK3 stably expressing HeLa cells were generated by transfecting FLAG-tagged human RIPK3 (pCI-neo plasmid) and selecting the cells with G418 (400 µg/ml). The cells were seeded at low density, and individual clones were isolated. Expression levels of FLAG-RIPK3 were examined by Western blotting, and a clone with no detectable RIPK3 expression was used as a negative control. Dox-inducible NBB_{140}-2xFV-VENUS or VENUS-expressing HeLa cells were generated by transfecting NBB_{140}-2xFV-VENUS or VENUS plasmids (pRetroX-TRE3G) with a standard retroviral transduction protocol and selecting the cells with G418 (500 µg/ml) and puromycin (2 µg/ml). The cells were seeded at a low density, and individual clones were isolated. Dox-induced expression of NBB_{140}-2xFV-VENUS and VENUS were confirmed by Western blotting.

Preparation of mouse tissue protein extracts

6- to 9-wk-old WT and *Ripk3*-deficient mice were euthanized by CO_2 inhalation followed by cervical dislocation. Liver, spleen, and cerebral cortex were homogenized using glass dounce homogenizers in an extraction buffer containing 20 mM Hepes, pH 7.4, 150 mM NaCl, 12.5 mM β-glycerophosphate, 1.5 mM $MgCl_2$, 2 mM EGTA, 10 mM NaF, 2 mM DTT, 1 mM Na_3VO_4, 1 mM phenylmethylsulfonyl fluoride, 20 µM aprotinin, and 0.5% Triton X-100. For preparation of protein extracts from intestinal enterocytes, duodenal (5 cm from the stomach) and ileal (5 cm above the cecum) small intestines were dissected, cut open, and washed with HBSS (Ca^{2+}/Mg^{2+}-free). The tissues were rinsed with HBSS (Ca^{2+}/Mg^{2+}-free) containing 1 mM DTT to remove mucosa. The tissues were transferred to 15 ml tubes with 10 ml of dissociation buffer (0.5 mM DTT and 1.5 mM EDTA in HBSS) and incubated for 30 min, at 4°C with rotation. After incubation, the tubes were vortex-mixed vigorously for 30 s, and the remaining tissues were removed. The tubes were centrifuged at 1,000 × *g* at 4°C for 10 min to collect the enterocytes. The cell pellets were resuspended in an extraction buffer described above, and proteins were extracted by sonication.

Oral infection of *Listeria* in mice

We used the previously reported method for oral transmission of *Listeria* (Bou Ghanem et al., 2012; D'Orazio, 2014). 6- to 9-wk-old female mice were food deprived for 16 h and fed with a 3–5-mm piece of white bread (Kroger) saturated with 5 µl of *Listeria* (10^8 colony-forming units [CFU]) in melted salted butter (Kroger). After the infection process, the mice were placed in a cage with raised wire flooring to prevent coprophagy, fed with regular chow, and housed for 3 d. The mice were then euthanized by CO_2 inhalation followed by cervical dislocation, and the whole liver was homogenized in 500 µl sterile H_2O. The homogenates were diluted and plated on BHI agar plates, which were incubated for 24–36 h at 37°C for enumeration of liver-colonizing *Listeria.*

Bacterial infection of cultured cells

Cells were seeded on 24-well plates at a concentration of $5 × 10^4$ cells per well on the day of infection. 4 h after plating, bacteria were added to the culture. For *Listeria* infection, the plates were centrifuged at 1,000 × *g* for 10 min at room temperature. The plates were incubated for 30 min at 37°C in 5% CO_2. The cells were then washed with sterile PBS and cultured in DMEM supplemented with 10% bovine growth serum and gentamicin

(100 µg/ml) for the indicated time periods. After the culture, the cells were washed with sterile PBS and lysed in PBS containing 0.2% Triton X-100. Serial dilutions of the lysates were spotted (10 µl/spot) on agar plates (BHI agar for *Listeria* and LB agar for *Salmonella* and *E. coli*) for enumeration of intracellular bacteria. For some experiments, GSK'872, NSA, or DMSO (vehicle) was added to the culture 30 min before the infection.

Western blotting

Protein extracts from cultured cells were prepared using an extraction buffer containing 20 mM Hepes, pH 7.4, 150 mM NaCl, 12.5 mM β-glycerophosphate, 1.5 mM MgCl$_2$, 2 mM EGTA, 10 mM NaF, 2 mM DTT, 1 mM Na$_3$VO$_4$, 1 mM phenylmethylsulfonyl fluoride, 20 µM aprotinin, and 0.5% Triton X-100. The extracts were boiled in SDS sample buffer containing 2-mercaptoethanol at 95°C for 5 min, resolved on SDS-PAGE, and transferred onto Hypond-P membranes (GE Healthcare). The membranes were immunoblotted with the indicated antibodies, and the bound antibodies were visualized with horseradish peroxidase–conjugated antibodies against rabbit or mouse IgG using the ECL Western blotting system (GE Healthcare).

For testing oligomerization of endogenous MLKL, protein extracts from cultured cells were boiled in 2-mercaptoethanol-free SDS sample buffer at 85°C for 10 min, and then resolved on SDS-PAGE.

Immunofluorescence microscopy analysis

For immunofluorescence staining of the mice liver, the whole liver was isolated and fixed with 4% paraformaldehyde. The fixed liver was embedded in optimum cutting temperature compound and frozen immediately. Cryosections (8 µm) were blocked with PBS containing 3% bovine serum albumin (Santa Cruz Biotechnology) for 30 min at room temperature and incubated with primary antibodies followed by incubation with anti-rabbit IgG conjugated with Alexa Fluor 594 and Alexa Fluor 488 phalloidin. For immunofluorescence staining of cultured cells, the cells were fixed with 10% formalin in PBS for 10 min, blocked with PBS containing 3% bovine serum albumin for 30 min at room temperature, and then incubated with primary antibodies followed by incubation with anti-rabbit IgG conjugated with Alexa 594 and anti-mouse IgG conjugated with Alexa Fluor 488 or Alexa Fluor 488 phalloidin. The samples were examined by a fluorescence microscope (model BX41; Olympus) and camera (model XM10; Olympus) at room temperature.

For Fig. 4 A, confocal images were obtained with a confocal microscope (LSM 880 with Airyscan; Carl Zeiss) using a 40×, NA = 1.2, water immersion objective, and images were collected with Zen Black 2.3 software (Carl Zeiss).

For Fig. S5 A, confocal images were obtained with a confocal microscope (FV-3000; Olympus) using a 60×, NA = 1.35, oil immersion objective, and images were collected with FV31S-DT software (Olympus). The images were exported as a full resolution TIF files and processed in Photoshop CC (Adobe) to adjust brightness and contrast.

Crystal violet assay and membrane permeability assay

Cells were seeded on 24-well plates at a concentration of 5×10^4 cells per well. The cells were either treated with TSQ or infected with *Listeria* for the indicated time periods. Floating dead cells were washed out with PBS, and adherent cells were fixed with 10% formalin in PBS.

For crystal violet assay, the cells were stained with 0.1% crystal violet. The dye was eluted in 50% ethanol and 0.1 M sodium citrate and analyzed at 595 nm using SmartSpecTM 3000 (Bio-Rad).

For membrane permeability assay, the cells were stained with ethidium homodimer III and Hoechst 33342. For quantification of membrane permeabilized cells, randomly photographed pictures for each sample were used. At smallest, <4,000 cells were analyzed for each sample, and total number of cells (Hoechst-positive) and number of membrane permeabilized cells (ethidium homodimer III–positive) were quantified using the ImageJ software. To calculate ratio of membrane permeabilized cells, the number of membrane-permeabilized cells was divided by the total cell number.

TUNEL staining of *Listeria*-invaded mouse enterocytes

6- to 9-wk-old female mice were food-deprived for 16 h and fed with a 3–5-mm piece of white bread (Kroger) saturated with 5 µl of *Listeria* (5×10^8 CFU) in melted salted butter (Kroger). After the infection process, the mice were placed in a cage with raised wire flooring to prevent coprophagy, fed with regular chow, and housed for 1 d. The mice were then euthanized by CO$_2$ inhalation followed by cervical dislocation, and ileum (5 cm above the cecum) was isolated. Luminal contents were washed out with PBS, and the tissues were fixed with 4% paraformaldehyde. The fixed ileum was embedded in paraffin wax. TUNEL staining of the tissue sections was conducted using the DeadEnd Fluorometric TUNEL System (Promega), followed by immunofluorescence staining of *Listeria*. For positive controls of TUNEL staining, 6-wk-old *Villin-CreER^T2, Tak1^flox/flox* mice were given intraperitoneal injections of tamoxifen (1 mg per mouse, ~20 g body weight, per day) for three consecutive days to induce *Tak1* gene deletion in the intestinal epithelial cells. The ileum was isolated at day 4 after the initiation of tamoxifen treatment.

Expression analysis of human *RIPK3* and *MLKL*

Human GTEx data were downloaded at the gene level from https://gtexportal.org/home/datasets (GTEx_Analysis_2016-01-15_v7_RNA-SeQCv1.1.8_gene_tpm.gct). These data consist of a matrix of transcripts per kilobase million normalized RNA-seq counts (56,202 Ensembl IDs by 11,688 samples). The counts associated with *RIPK3* and *MLKL* (no. ENSG00000129465 and ENSG00000168404, respectively) were summarized across tissues and inversely ordered by median expression levels for visualization purposes.

In vitro NBB$_{140}$-2xFV-VENUS binding assay and growth inhibition assay of bacteria

Dox-inducible VENUS and NBB$_{140}$-2xFV-VENUS expressing HeLa cells were treated with Dox (1 µg/ml) for 6 h. The cells were resuspended in H$_2$O containing protease inhibitor (Protease Arrest; Calbiochem), and proteins were extracted by sonication. The extracts were incubated with either ethanol (vehicle) or DIM (25 nM) at 4°C for 1 h. To confirm oligomerization of NBB$_{140}$-2xFV-VENUS upon DIM treatment, disuccinimidyl suberate (5 mM) was added to aliquots of the extracts and analyzed by Western blotting.

For NBB$_{140}$-2xFV-VENUS binding assay, 40 µl of 5× bacterial growth medium and bacteria (10^8 CFU) were added to 160 µl of the extracts, and the mixture was incubated for 1 h at 37°C. After incubation, the bacteria were precipitated by centrifugation at 5,000 × g for 10 min, washed twice with PBS, and boiled in SDS sample buffer. The extracts were resolved on SDS-PAGE, and coprecipitated proteins were analyzed by Western blotting.

For growth inhibition assay, 40 µl of 5× bacterial growth medium and bacteria (2 × 10^2 CFU) were added to 160 µl of the extracts, and the mixture was incubated for 2 h at 37°C. After incubation, serial dilutions of the culture were spotted (10 µl/spot) on agar plates (BHI agar for *Listeria* and LB agar for *Salmonella* and *E. coli*) for enumeration of bacteria.

EM analysis of *Listeria*

Dox-inducible VENUS and NBB$_{140}$-2xFV-VENUS expressing HeLa cells were treated with Dox (1 µg/ml) for 6 h. The cells were resuspended in H$_2$O containing protease inhibitor, and proteins were extracted by sonication. 60 µl of 5× BHI broth and *Listeria* (10^8 CFU) were added to 540 µl of the extracts, and the mixture was incubated for 1 h at 37°C. After incubation, the *Listeria* was precipitated by centrifugation at 19,000 × g for 3 min, washed twice with PBS, and fixed in Karnovsky's fixative, 2% paraformaldehyde (EM grade; Electron Microscopy Sciences), and 2.5% glutaraldehyde (EM grade; Electron Microscopy Sciences) in PBS overnight at 4°C. The *Listeria* was centrifuged for 5 min and rinsed in three 30-min changes of cold 0.1 M cacodylate buffer, pH 7.4, and then post-fixed in 2% OsO$_4$ in the same buffer for 1 h at 4°C in the dark, and rinsed three times as above. The *Listeria* was preembedded in 2% agarose prepared in 0.1 M cacodylate buffer, pH 7.4. Samples were dehydrated in a graded series of ethanol (30%, 50%, 70%, 95%, and 3× 100%) followed by infiltration with Spurr's resin and embedding in BEEM capsules at 70°C. Cured blocks were trimmed, thin-sectioned at 80 nm, and collected on Formvar/carbon grids, and all grids were stained with 4% aqueous uranyl acetate and Reynold's lead citrate before viewing on a JEM-1200EX TEM (JEOL USA) fitted with a Gatan ES1000W digital camera.

Statistical analyses

Statistical analyses were performed using the one-way ANOVA with Tukey's multiple comparisons test, or the unpaired Student's t test (two-tailed) with equal distributions. *, $P < 0.05$; **, $P < 0.01$; ***, $P < 0.001$; ****, $P < 0.0001$; NS when $P \geqq 0.05$.

Online supplemental material

Fig. S1 shows expression analysis of *RIPK3* and *MLKL* in multiple human tissues. Fig. S2 shows *Listeria* number in control and RIPK3-expressing HeLa cells at 2 hpi, MLKL activation by *Salmonella* infection, and *Salmonella* replication in control and RIPK3-expressing HeLa cells. Fig. S3 shows TUNEL staining of *Listeria*-infected intestinal epithelium. Fig. S4 shows necroptosis induction in *Listeria*-infected cells. Fig. S5 shows membrane localization of MLKL in TSQ-treated and *Listeria*-infected HT-29 cells, and interaction between NBB$_{140}$-2xFV and *Listeria*, *Salmonella*, and *E. coli*.

References

Abreu, M.T. 2010. Toll-like receptor signalling in the intestinal epithelium: how bacterial recognition shapes intestinal function. *Nat. Rev. Immunol.* 10:131–144. https://doi.org/10.1038/nri2707

Bauckman, K.A., N. Owusu-Boaitey, and I.U. Mysorekar. 2015. Selective autophagy: xenophagy. *Methods.* 75:120–127. https://doi.org/10.1016/j.ymeth.2014.12.005

Bischofberger, M., M.R. Gonzalez, and F.G. van der Goot. 2009. Membrane injury by pore-forming proteins. *Curr. Opin. Cell Biol.* 21:589–595. https://doi.org/10.1016/j.ceb.2009.04.003

Blériot, C., T. Dupuis, G. Jouvion, G. Eberl, O. Disson, and M. Lecuit. 2015. Liver-resident macrophage necroptosis orchestrates type 1 microbicidal inflammation and type-2-mediated tissue repair during bacterial infection. *Immunity.* 42:145–158. https://doi.org/10.1016/j.immuni.2014.12.020

Bou Ghanem, E.N., G.S. Jones, T. Myers-Morales, P.D. Patil, A.N. Hidayatullah, and S.E. D'Orazio. 2012. InlA promotes dissemination of Listeria monocytogenes to the mesenteric lymph nodes during food borne infection of mice. *PLoS Pathog.* 8:e1003015. https://doi.org/10.1371/journal.ppat.1003015

Brogden, K.A. 2005. Antimicrobial peptides: pore formers or metabolic inhibitors in bacteria? *Nat. Rev. Microbiol.* 3:238–250. https://doi.org/10.1038/nrmicro1098

Cai, Z., S. Jitkaew, J. Zhao, H.-C. Chiang, S. Choksi, J. Liu, Y. Ward, L.G. Wu, and Z.-G. Liu. 2014. Plasma membrane translocation of trimerized MLKL protein is required for TNF-induced necroptosis. *Nat. Cell Biol.* 16:55–65. https://doi.org/10.1038/ncb2883

Cemma, M., and J.H. Brumell. 2012. Interactions of pathogenic bacteria with autophagy systems. *Curr. Biol.* 22:R540–R545. https://doi.org/10.1016/j.cub.2012.06.001

D'Orazio, S.E. 2014. Animal models for oral transmission of Listeria monocytogenes. *Front. Cell. Infect. Microbiol.* 4:15. https://doi.org/10.3389/fcimb.2014.00015

Dalebroux, Z.D., M.B. Edrozo, R.A. Pfuetzner, S. Ressl, B.R. Kulasekara, M.P. Blanc, and S.I. Miller. 2015. Delivery of cardiolipins to the Salmonella outer membrane is necessary for survival within host tissues and virulence. *Cell Host Microbe.* 17:441–451. https://doi.org/10.1016/j.chom.2015.03.003

Daniels, B.P., A.G. Snyder, T.M. Olsen, S. Orozco, T.H. Oguin III, S.W.G. Tait, J. Martinez, M. Gale Jr., Y.M. Loo, and A. Oberst. 2017. RIPK3 restricts viral pathogenesis via cell death-independent neuroinflammation. *Cell.* 169:301–313.e11.

Demchick, P., and A.L. Koch. 1996. The permeability of the wall fabric of Escherichia coli and Bacillus subtilis. *J. Bacteriol.* 178:768–773. https://doi.org/10.1128/jb.178.3.768-773.1996

Deretic, V., T. Saitoh, and S. Akira. 2013. Autophagy in infection, inflammation and immunity. *Nat. Rev. Immunol.* 13:722–737. https://doi.org/10.1038/nri3532

Ding, J., K. Wang, W. Liu, Y. She, Q. Sun, J. Shi, H. Sun, D.C. Wang, and F. Shao. 2016. Pore-forming activity and structural autoinhibition of the gasdermin family. *Nature.* 535:111–116. https://doi.org/10.1038/nature18590

do Nascimento, V.V., É.O. Mello, L.P. Carvalho, E.J. de Melo, A.O. Carvalho, K.V. Fernandes, and V.M. Gomes. 2015. PvD1 defensin, a plant antimicrobial peptide with inhibitory activity against Leishmania amazonensis. *Biosci. Rep.* 35:e00248. https://doi.org/10.1042/BSR20150060

Dondelinger, Y., W. Declercq, S. Montessuit, R. Roelandt, A. Goncalves, I. Bruggeman, P. Hulpiau, K. Weber, C.A. Sehon, R.W. Marquis, et al. 2014. MLKL compromises plasma membrane integrity by binding to phosphatidylinositol phosphates. *Cell Reports.* 7:971–981. https://doi.org/10.1016/j.celrep.2014.04.026

Downey, J., E. Pernet, F. Coulombe, B. Allard, I. Meunier, J. Jaworska, S. Qureshi, D.C. Vinh, J.G. Martin, P. Joubert, and M. Divangahi. 2017. RIPK3 interacts with MAVS to regulate type I IFN-mediated immunity to Influenza A virus infection. *PLoS Pathog.* 13:e1006326. https://doi.org/10.1371/journal.ppat.1006326

Epand, R.M., and R.F. Epand. 2009. Lipid domains in bacterial membranes and the action of antimicrobial agents. *Biochim. Biophys. Acta.* 1788:289–294. https://doi.org/10.1016/j.bbamem.2008.08.023

Ernst, W.A., S. Thoma-Uszynski, R. Teitelbaum, C. Ko, D.A. Hanson, C. Clayberger, A.M. Krensky, M. Leippe, B.R. Bloom, T. Ganz, and R.L. Modlin. 2000. Granulysin, a T cell product, kills bacteria by altering membrane permeability. *J. Immunol.* 165:7102–7108. https://doi.org/10.4049/jimmunol.165.12.7102

Ganz, T. 2003. Defensins: antimicrobial peptides of innate immunity. *Nat. Rev. Immunol.* 3:710–720. https://doi.org/10.1038/nri1180

González-Juarbe, N., R.P. Gilley, C.A. Hinojosa, K.M. Bradley, A. Kamei, G. Gao, P.H. Dube, M.A. Bergman, and C.J. Orihuela. 2015. Pore-forming toxins induce macrophage necroptosis during acute bacterial pneumonia. *PLoS Pathog.* 11:e1005337. https://doi.org/10.1371/journal.ppat.1005337

Goodall, M.L., B.E. Fitzwalter, S. Zahedi, M. Wu, D. Rodriguez, J.M. Mulcahy-Levy, D.R. Green, M. Morgan, S.D. Cramer, and A. Thorburn. 2016. The autophagy machinery controls cell death switching between apoptosis and necroptosis. *Dev. Cell.* 37:337–349. https://doi.org/10.1016/j.devcel.2016.04.018

GTEx Consortium. 2013. The Genotype-Tissue Expression (GTEx) project. *Nat. Genet.* 45:580–585. https://doi.org/10.1038/ng.2653

Harris, K.G., S.A. Morosky, C.G. Drummond, M. Patel, C. Kim, D.B. Stolz, J.M. Bergelson, S. Cherry, and C.B. Coyne. 2015. RIP3 regulates autophagy and promotes coxsackievirus B3 infection of intestinal epithelial cells. *Cell Host Microbe.* 18:221–232. https://doi.org/10.1016/j.chom.2015.07.007

Hartmann, B.M., R.A. Albrecht, E. Zaslavsky, G. Nudelman, H. Pincas, N. Marjanovic, M. Schotsaert, C. Martínez-Romero, R. Fenutria, J.P. Ingram, et al. 2017. Pandemic H1N1 influenza A viruses suppress immunogenic RIPK3-driven dendritic cell death. *Nat. Commun.* 8:1931. https://doi.org/10.1038/s41467-017-02035-9

Havell, E.A. 1986. Synthesis and secretion of interferon by murine fibroblasts in response to intracellular Listeria monocytogenes. *Infect. Immun.* 54:787–792.

Holmgren, J., and C. Czerkinsky. 2005. Mucosal immunity and vaccines. *Nat. Med.* 11(4 Suppl):S45–S53. https://doi.org/10.1038/nm1213

Huang, J., V. Canadien, G.Y. Lam, B.E. Steinberg, M.C. Dinauer, M.A. Magalhaes, M. Glogauer, S. Grinstein, and J.H. Brumell. 2009. Activation of antibacterial autophagy by NADPH oxidases. *Proc. Natl. Acad. Sci. USA.* 106:6226–6231. https://doi.org/10.1073/pnas.0811045106

Jo, E.-K., J.K. Kim, and S. Hwang. 2016. Xenophagy: Autophagy in direct pathogen elimination. *In* Autophagy Networks in Inflammation. M.C. Maiuri and D. De Stefano, editors. Springer International Publishing, Cham, Switzerland. 135–153. https://doi.org/10.1007/978-3-319-30079-5_7

Kajino-Sakamoto, R., E. Omori, P.K. Nighot, A.T. Blikslager, K. Matsumoto, and J. Ninomiya-Tsuji. 2010. TGF-β-activated kinase 1 signaling maintains intestinal integrity by preventing accumulation of reactive oxygen species in the intestinal epithelium. *J. Immunol.* 185:4729–4737. https://doi.org/10.4049/jimmunol.0903587

Kawai, T., and S. Akira. 2010. The role of pattern-recognition receptors in innate immunity: update on Toll-like receptors. *Nat. Immunol.* 11:373–384. https://doi.org/10.1038/ni.1863

Kayagaki, N., I.B. Stowe, B.L. Lee, K. O'Rourke, K. Anderson, S. Warming, T. Cuellar, B. Haley, M. Roose-Girma, Q.T. Phung, et al. 2015. Caspase-11 cleaves gasdermin D for non-canonical inflammasome signalling. *Nature.* 526:666–671. https://doi.org/10.1038/nature15541

Koo, G.B., M.J. Morgan, D.G. Lee, W.J. Kim, J.H. Yoon, J.S. Koo, S.I. Kim, S.J. Kim, M.K. Son, S.S. Hong, et al. 2015. Methylation-dependent loss of RIP3 expression in cancer represses programmed necrosis in response to chemotherapeutics. *Cell Res.* 25:707–725. https://doi.org/10.1038/cr.2015.56

Krokowski, S., D. Lobato-Marquez, A. Chastanet, P.M. Pereira, D. Angelis, D. Galea, G. Larrouy-Maumus, R. Henriques, E.T. Spiliotis, R. Carballido-Lopez, et al. 2018. Septins recognize and entrap dividing bacterial cells for delivery to lysosomes. *Cell Host Microbe.* 24:866–874.e4.

Kumar, H., T. Kawai, and S. Akira. 2009. Toll-like receptors and innate immunity. *Biochem. Biophys. Res. Commun.* 388:621–625. https://doi.org/10.1016/j.bbrc.2009.08.062

Lambert, P.A. 2002. Cellular impermeability and uptake of biocides and antibiotics in Gram-positive bacteria and mycobacteria. *J. Appl. Microbiol.* 92(s1, Suppl):46S–54S. https://doi.org/10.1046/j.1365-2672.92.5s1.7.x

Lawlor, K.E., N. Khan, A. Mildenhall, M. Gerlic, B.A. Croker, A.A. D'Cruz, C. Hall, S. Kaur Spall, H. Anderton, S.L. Masters, et al. 2015. RIPK3 promotes cell death and NLRP3 inflammasome activation in the absence of MLKL. *Nat. Commun.* 6:6282. https://doi.org/10.1038/ncomms7282

Lecuit, M. 2007. Human listeriosis and animal models. *Microbes Infect.* 9:1216–1225. https://doi.org/10.1016/j.micinf.2007.05.009

Lecuit, M., S. Vandormael-Pournin, J. Lefort, M. Huerre, P. Gounon, C. Dupuy, C. Babinet, and P. Cossart. 2001. A transgenic model for listeriosis: role of internalin in crossing the intestinal barrier. *Science.* 292:1722–1725. https://doi.org/10.1126/science.1059852

Lieberman, J. 2003. The ABCs of granule-mediated cytotoxicity: new weapons in the arsenal. *Nat. Rev. Immunol.* 3:361–370. https://doi.org/10.1038/nri1083

Linkermann, A., and D.R. Green. 2014. Necroptosis. *N. Engl. J. Med.* 370:455–465. https://doi.org/10.1056/NEJMra1310050

Liu, X., Z. Zhang, J. Ruan, Y. Pan, V.G. Magupalli, H. Wu, and J. Lieberman. 2016. Inflammasome-activated gasdermin D causes pyroptosis by forming membrane pores. *Nature.* 535:153–158. https://doi.org/10.1038/nature18629

Mariathasan, S., and D.M. Monack. 2007. Inflammasome adaptors and sensors: intracellular regulators of infection and inflammation. *Nat. Rev. Immunol.* 7:31–40. https://doi.org/10.1038/nri1997

McCaffrey, R.L., P. Fawcett, M. O'Riordan, K.D. Lee, E.A. Havell, P.O. Brown, and D.A. Portnoy. 2004. A specific gene expression program triggered by Gram-positive bacteria in the cytosol. *Proc. Natl. Acad. Sci. USA.* 101:11386–11391. https://doi.org/10.1073/pnas.0403215101

McCollum, J.T., A.B. Cronquist, B.J. Silk, K.A. Jackson, K.A. O'Connor, S. Cosgrove, J.P. Gossack, S.S. Parachini, N.S. Jain, P. Ettestad, et al. 2013. Multistate outbreak of listeriosis associated with cantaloupe. *N. Engl. J. Med.* 369:944–953. https://doi.org/10.1056/NEJMoa1215837

McLauchlin, J., R.T. Mitchell, W.J. Smerdon, and K. Jewell. 2004. Listeria monocytogenes and listeriosis: a review of hazard characterisation for use in microbiological risk assessment of foods. *Int. J. Food Microbiol.* 92:15–33. https://doi.org/10.1016/S0168-1605(03)00326-X

Melton-Witt, J.A., S.M. Rafelski, D.A. Portnoy, and A.I. Bakardjiev. 2012. Oral infection with signature-tagged Listeria monocytogenes reveals organ-specific growth and dissemination routes in guinea pigs. *Infect. Immun.* 80:720–732. https://doi.org/10.1128/IAI.05958-11

Meylan, E., J. Tschopp, and M. Karin. 2006. Intracellular pattern recognition receptors in the host response. *Nature.* 442:39–44. https://doi.org/10.1038/nature04946

Moriwaki, K., J. Bertin, P.J. Gough, G.M. Orlowski, and F.K. Chan. 2015. Differential roles of RIPK1 and RIPK3 in TNF-induced necroptosis and chemotherapeutic agent-induced cell death. *Cell Death Dis.* 6:e1636. https://doi.org/10.1038/cddis.2015.16

Murphy, J.M., P.E. Czabotar, J.M. Hildebrand, I.S. Lucet, J.G. Zhang, S. Alvarez-Diaz, R. Lewis, N. Lalaoui, D. Metcalf, A.I. Webb, et al. 2013. The pseudokinase MLKL mediates necroptosis via a molecular switch mechanism. *Immunity.* 39:443–453. https://doi.org/10.1016/j.immuni.2013.06.018

Najjar, M., D. Saleh, M. Zelic, S. Nogusa, S. Shah, A. Tai, J.N. Finger, A. Polykratis, P.J. Gough, J. Bertin, et al. 2016. RIPK1 and RIPK3 kinases promote cell-death-independent inflammation by Toll-like receptor 4. *Immunity.* 45:46–59. https://doi.org/10.1016/j.immuni.2016.06.007

Newton, K., X. Sun, and V.M. Dixit. 2004. Kinase RIP3 is dispensable for normal NF-kappa Bs, signaling by the B-cell and T-cell receptors, tumor necrosis factor receptor 1, and Toll-like receptors 2 and 4. *Mol. Cell. Biol.* 24:1464–1469. https://doi.org/10.1128/MCB.24.4.1464-1469.2004

Newton, K., D.L. Dugger, A. Maltzman, J.M. Greve, M. Hedehus, B. Martin-McNulty, R.A. Carano, T.C. Cao, N. van Bruggen, L. Bernstein, et al. 2016. RIPK3 deficiency or catalytically inactive RIPK1 provides greater benefit than MLKL deficiency in mouse models of inflammation and tissue injury. *Cell Death Differ.* 23:1565–1576. https://doi.org/10.1038/cdd.2016.46

Niemann, H.H., V. Jäger, P.J. Butler, J. van den Heuvel, S. Schmidt, D. Ferraris, E. Gherardi, and D.W. Heinz. 2007. Structure of the human receptor tyrosine kinase met in complex with the Listeria invasion protein InlB. *Cell.* 130:235–246. https://doi.org/10.1016/j.cell.2007.05.037

Pasparakis, M., and P. Vandenabeele. 2015. Necroptosis and its role in inflammation. *Nature.* 517:311–320. https://doi.org/10.1038/nature14191

Perez-Lopez, A., J. Behnsen, S.P. Nuccio, and M. Raffatellu. 2016. Mucosal immunity to pathogenic intestinal bacteria. *Nat. Rev. Immunol.* 16:135–148. https://doi.org/10.1038/nri.2015.17

Philpott, D.J., S. Yamaoka, A. Israël, and P.J. Sansonetti. 2000. Invasive Shigella flexneri activates NF-κ B through a lipopolysaccharide-dependent innate intracellular response and leads to IL-8 expression in epithelial cells. *J. Immunol.* 165:903–914. https://doi.org/10.4049/jimmunol.165.2.903

Quarato, G., C.S. Guy, C.R. Grace, F. Llambi, A. Nourse, D.A. Rodriguez, R. Wakefield, S. Frase, T. Moldoveanu, and D.R. Green. 2016. Sequential engagement of distinct MLKL phosphatidylinositol-binding sites executes necroptosis. *Mol. Cell.* 61:589–601. https://doi.org/10.1016/j.molcel.2016.01.011

Rodriguez, D.A., R. Weinlich, S. Brown, C. Guy, P. Fitzgerald, C.P. Dillon, A. Oberst, G. Quarato, J. Low, J.G. Cripps, et al. 2016. Characterization of RIPK3-mediated phosphorylation of the activation loop of MLKL during necroptosis. *Cell Death Differ.* 23:76–88. https://doi.org/10.1038/cdd.2015.70

Sanjuan, M.A., C.P. Dillon, S.W. Tait, S. Moshiach, F. Dorsey, S. Connell, M. Komatsu, K. Tanaka, J.L. Cleveland, S. Withoff, and D.R. Green. 2007. Toll-like receptor signalling in macrophages links the autophagy pathway to phagocytosis. *Nature.* 450:1253–1257. https://doi.org/10.1038/nature06421

Schlame, M., D. Rua, and M.L. Greenberg. 2000. The biosynthesis and functional role of cardiolipin. *Prog. Lipid Res.* 39:257–288. https://doi.org/10.1016/S0163-7827(00)00005-9

Schubert, W.D., C. Urbanke, T. Ziehm, V. Beier, M.P. Machner, E. Domann, J. Wehland, T. Chakraborty, and D.W. Heinz. 2002. Structure of internalin, a major invasion protein of Listeria monocytogenes, in complex with its human receptor E-cadherin. *Cell.* 111:825–836. https://doi.org/10.1016/S0092-8674(02)01136-4

Sorbara, M.T., and S.E. Girardin. 2015. Emerging themes in bacterial autophagy. *Curr. Opin. Microbiol.* 23:163–170. https://doi.org/10.1016/j.mib.2014.11.020

Speert, D.P., L.W. Wannamaker, E.D. Gray, and C.C. Clawson. 1979. Bactericidal effect of oleic acid on group A streptococci: mechanism of action. *Infect. Immun.* 26:1202–1210.

Su, Z., Z. Yang, L. Xie, J.P. DeWitt, and Y. Chen. 2016. Cancer therapy in the necroptosis era. *Cell Death Differ.* 23:748–756. https://doi.org/10.1038/cdd.2016.8

Sun, L., H. Wang, Z. Wang, S. He, S. Chen, D. Liao, L. Wang, J. Yan, W. Liu, X. Lei, and X. Wang. 2012. Mixed lineage kinase domain-like protein mediates necrosis signaling downstream of RIP3 kinase. *Cell.* 148:213–227. https://doi.org/10.1016/j.cell.2011.11.031

Thapa, R.J., J.P. Ingram, K.B. Ragan, S. Nogusa, D.F. Boyd, A.A. Benitez, H. Sridharan, R. Kosoff, M. Shubina, V.J. Landsteiner, et al. 2016. DAI Senses Influenza A Virus Genomic RNA and Activates RIPK3-Dependent Cell Death. *Cell Host Microbe.* 20:674–681. https://doi.org/10.1016/j.chom.2016.09.014

Thiagarajah, J.R., M. Donowitz, and A.S. Verkman. 2015. Secretory diarrhoea: mechanisms and emerging therapies. *Nat. Rev. Gastroenterol. Hepatol.* 12:446–457. https://doi.org/10.1038/nrgastro.2015.111

Thurston, T.L., M.P. Wandel, N. von Muhlinen, A. Foeglein, and F. Randow. 2012. Galectin 8 targets damaged vesicles for autophagy to defend cells against bacterial invasion. *Nature.* 482:414–418. https://doi.org/10.1038/nature10744

Trapani, J.A., and M.J. Smyth. 2002. Functional significance of the perforin/granzyme cell death pathway. *Nat. Rev. Immunol.* 2:735–747. https://doi.org/10.1038/nri911

Travassos, L.H., L.A.M. Carneiro, M. Ramjeet, S. Hussey, Y.-G. Kim, J.G. Magalhães, L. Yuan, F. Soares, E. Chea, L. Le Bourhis, et al. 2010. Nod1 and Nod2 direct autophagy by recruiting ATG16L1 to the plasma membrane at the site of bacterial entry. *Nat. Immunol.* 11:55–62. https://doi.org/10.1038/ni.1823

Upton, J.W., and W.J. Kaiser. 2017. DAI another way: Necroptotic control of viral infection. *Cell Host Microbe.* 21:290–293. https://doi.org/10.1016/j.chom.2017.01.016

Upton, J.W., W.J. Kaiser, and E.S. Mocarski. 2010. Virus inhibition of RIP3-dependent necrosis. *Cell Host Microbe.* 7:302–313. https://doi.org/10.1016/j.chom.2010.03.006

Upton, J.W., W.J. Kaiser, and E.S. Mocarski. 2012. DAI/ZBP1/DLM-1 complexes with RIP3 to mediate virus-induced programmed necrosis that is targeted by murine cytomegalovirus vIRA. *Cell Host Microbe.* 11:290–297. https://doi.org/10.1016/j.chom.2012.01.016

Walch, M., F. Dotiwala, S. Mulik, J. Thiery, T. Kirchhausen, C. Clayberger, A.M. Krensky, D. Martinvalet, and J. Lieberman. 2014. Cytotoxic cells kill intracellular bacteria through granulysin-mediated delivery of granzymes. *Cell.* 157:1309–1323. https://doi.org/10.1016/j.cell.2014.03.062

Wang, H., L. Sun, L. Su, J. Rizo, L. Liu, L.F. Wang, F.S. Wang, and X. Wang. 2014. Mixed lineage kinase domain-like protein MLKL causes necrotic membrane disruption upon phosphorylation by RIP3. *Mol. Cell.* 54:133–146. https://doi.org/10.1016/j.molcel.2014.03.003

Wang, Q., M. Yu, K. Zhang, J. Liu, P. Tao, S. Ge, and Z. Ning. 2016. Expression profile and tissue-specific distribution of the receptor-interacting protein 3 in BALB/c Mice. *Biochem. Genet.* 54:360–367. https://doi.org/10.1007/s10528-016-9724-2

Wu, J., Z. Huang, J. Ren, Z. Zhang, P. He, Y. Li, J. Ma, W. Chen, Y. Zhang, X. Zhou, et al. 2013. Mlkl knockout mice demonstrate the indispensable role of Mlkl in necroptosis. *Cell Res.* 23:994–1006. https://doi.org/10.1038/cr.2013.91

Xia, B., S. Fang, X. Chen, H. Hu, P. Chen, H. Wang, and Z. Gao. 2016. MLKL forms cation channels. *Cell Res.* 26:517–528. https://doi.org/10.1038/cr.2016.26

Youle, R.J., and A. Strasser. 2008. The BCL-2 protein family: opposing activities that mediate cell death. *Nat. Rev. Mol. Cell Biol.* 9:47–59. https://doi.org/10.1038/nrm2308

Zhang, Y.M., and C.O. Rock. 2008. Membrane lipid homeostasis in bacteria. *Nat. Rev. Microbiol.* 6:222–233. https://doi.org/10.1038/nrmicro1839